Journal of Applied Physics

Scattering by lossy anisotropic scatterers: A modal approach

Cite as: J. Appl. Phys. **129**, 113104 (2021); https://doi.org/10.1063/5.0039134
Submitted: 30 November 2020 • Accepted: 24 February 2021 • Published Online: 19 March 2021

N. Kossowski, Parry Y. Chen, Q. J. Wang, et al.

COLLECTIONS

Paper published as part of the special topic on Plasmonics: Enabling Functionalities with Novel Materials

This paper was selected as Featured

This paper was selected as Scilight

View Online Export Citation CrossMark

ARTICLES YOU MAY BE INTERESTED IN

Principles, technologies, and applications of plasmonic biosensors
Journal of Applied Physics **129**, 111102 (2021); https://doi.org/10.1063/5.0042811

Imaging ellipsometry for structured and plasmonic materials
Journal of Applied Physics **129**, 113101 (2021); https://doi.org/10.1063/5.0039150

A plasmonically enhanced route to faster and more energy-efficient phase-change integrated photonic memory and computing devices
Journal of Applied Physics **129**, 110902 (2021); https://doi.org/10.1063/5.0042962

Learn More
Journal of Applied Physics Special Topics Open for Submissions

AIP Publishing

© 2021 Author(s).

Journal of Applied Physics ARTICLE scitation.org/journal/jap

Scattering by lossy anisotropic scatterers: A modal approach

Cite as: J. Appl. Phys. **129**, 113104 (2021); doi: 10.1063/5.0039134
Submitted: 30 November 2020 · Accepted: 24 February 2021 ·
Published Online: 19 March 2021

View Online Export Citation CrossMark

N. Kossowski,[1,2,a)] Parry Y. Chen,[3] Q. J. Wang,[1,2,4] P. Genevet,[5] and Yonatan Sivan[3,a)]

AFFILIATIONS

[1]UMI 3288 CINTRA, CNRS/NTU/THALES, Nanyang Technological University, Research Techno Plaza, 50 Nanyang Drive, Singapore 637553
[2]School of Electronic and Electrical Engineering, Nanyang Technological University, 50 Nanyang Ave., Singapore 639798
[3]School of Electrical and Computer Engineering, Ben-Gurion University, Beer-Sheva, Israel
[4]School of Physical and Mathematical Sciences, Nanyang Technological University, 50 Nanyang Ave., Singapore 639798
[5]CNRS-Centre de Recherche sur l'Hetero-Epitaxie et ses Applications, Universite Cote d'Azur, Rue Bernard Gregory, Sophia-Antipolis, Valbonne, 06560, France

Note: This paper is part of the Special Topic on Plasmonics: Enabling Functionalities with Novel Materials.
[a)]**Authors to whom correspondence should be addressed:** koss0001@e.ntu.edu.sg **and** sivanyon@bgu.ac.il

ABSTRACT

Scattering from anisotropic geometries of arbitrary shape is relatively difficult to interpret physically, involving the intricate interplay between material and geometric effects. Insights into complex scattering mechanisms are often enabled by modal methods that decompose the response into the well-understood multipolar resonances. Here, we extend the generalized normal mode expansion to lossy and anisotropic scatterers. Unique to the method is that it decomposes the total response of any anisotropic resonator into the modes of the corresponding isotropic resonator. This disentangles the material and geometric contributions to the scattering of any anisotropic resonator. Furthermore, the method can identify absorption and scattering resonances with separate sets of modes. We illustrate our method by considering an infinitely long cylinder with concentric metallic/dielectric layers, targeting the complex case of an effective hyperbolic response. We show that by scanning the material composition of the hyperbolic medium, we can achieve any desired scattering effect, including backscattering cancellation.

Published under license by AIP Publishing. https://doi.org/10.1063/5.0039134

I. INTRODUCTION

With the recent developments of metamaterials and metasurfaces, it has become imperative to develop new tools to understand the absorption and scattering properties of composite material nanoparticles.[1–6] Assuming that the geometric parameters of the composite are small compared to the wavelength of the excitation wave, such materials can usually be described by a unique homogeneous anisotropic permittivity tensor.[7,8] To develop such a tool, it is simpler but nevertheless challenging to begin with the study of two-dimensional scatterers with tensorial dielectric function.

Electromagnetic scattering by anisotropic cylinders is an old problem,[9] which has been extensively investigated. Many solutions have been developed, including integral solutions for circular cylinders,[10,11] a variational approach,[12] surface integrals,[13,14] Fourier domain,[15] and coupled-dipole approximation.[16] For the most complex cases, like lossy cylinders of arbitrary shape, some integral solutions have been proposed[17,18] or one may still rely on finite differences time-domain (FDTD)[19] and finite element methods[20] to extract the optical properties of complex nanostructures. Although these methods are generally applicable, they do not provide physical insight into the resonant modes that are excited within the structure. Such modal decompositions for arbitrary materials have been developed only for simple geometries (e.g., circular cross section), where an exact expression for the eigenmodes is available in terms of vector cylindrical harmonics.[21,22]

More recently, it was shown that resonant states[23] or quasi-normal modes[24,25] may provide another route to obtaining a modal decomposition in the case of lossy (i.e., non-conservative) systems.

Published under license by AIP Publishing.

These modes have to be introduced to describe the radiative loss of the system to the background[26] as well as any absorption losses. They are solutions of the source-free Helmholtz equation with complex eigenfrequencies. Although this formalism allows the treatment of anisotropic[27,28] and bi-anisotropic materials,[29] those modes form a complete basis inside the inclusion only, and outside, their amplitudes diverge exponentially. This divergence can be managed by taking into account the causality principle,[30,31] by redefining the normalization based on perturbation theory[23] or by enclosing the resonant structure by a perfectly matched layer.[28] However, the implementation of these techniques requires skill and experience to avoid spurious and missing modes and is frequently slower than a solution of the scattering problem itself.[25,32]

Alternatively, instead of setting frequency to be the eigenvalue for the source-free Helmholtz equation, we may set the eigenvalue to be one of the material properties of the inclusion, yielding eigenpermittivities[33] or eigenconductivities.[34] This generates a new orthogonal set of modes that decay rather than grow outside the structure and have a simple normalization.[32] These modes have been widely used.[35–40] For simple geometries (e.g., a slab, cylinder, sphere), analytical solutions of the eigenmodes are available,[32,34,36–38,40–47] along with an efficient complex root search for the eigenvalues.[43] For more complicated geometries, one can always resort to a numerical approach.[32,41] Clusters of scatterers can be treated with minimal overhead computations by the rigorous hybridization approach described in Refs. 48, 45, and 34.

The generalized normal mode expansion (GENOME)[32] uses the eigenpermittivity modes to derive a modal decomposition of the scattering of lossy open-systems in the case of isotropic materials. In this paper, we extend GENOME to the case of anisotropic materials. We show how the modes of anisotropic structures can be obtained by expanding in terms of modes of an isotropic inclusion.[42] We validate our method by comparing our results to Mie theory.[49,50] Our method is then exploited to perform a modal analysis of the scattering from an infinite hyperbolic metamaterial cylinder with concentric metal/dielectric layers. By considering the coherent superposition of the scattered modes, new physical insight is revealed regarding the radiation properties of such structures, and we demonstrate how such materials can play an important role in the design of complex scattering functionalities, such as backscattering cancellation. This work will be the basis for the implementation of the method to more complicated anisotropic structures.

II. GENERALIZED NORMAL MODE EXPANSION

We consider an inclusion with an anisotropic material of permittivity $\overleftrightarrow{\varepsilon}_i$ embedded in an isotropic medium ε_b illuminated by an incident monochromatic wave $\boldsymbol{E}_0$ [see Fig. 1(a)]. We can express the vector Helmholtz equation that governs its evolution over all space by introducing the indicator function $\theta(\boldsymbol{r})$ that is 1 inside the inclusion and 0 outside [see Fig. 1(b)],

$$\nabla \times \nabla \times \boldsymbol{E}(\boldsymbol{r}) - k^2 \varepsilon_b \boldsymbol{E}(\boldsymbol{r}) = i\omega\mu_0 \boldsymbol{J}(\boldsymbol{r}) + k^2 \theta(\boldsymbol{r})\, \Delta\overleftrightarrow{\varepsilon}\, \boldsymbol{E}(\boldsymbol{r}), \quad (1)$$

where $\Delta\overleftrightarrow{\varepsilon} = \overleftrightarrow{\varepsilon}_i - \varepsilon_b$ is the contrast in permittivity between the inclusion and the background. This contrast induces a polarization current density inside the inclusion, $k^2\theta(\boldsymbol{r})\Delta\overleftrightarrow{\varepsilon}\boldsymbol{E}(\boldsymbol{r})$. Introducing the

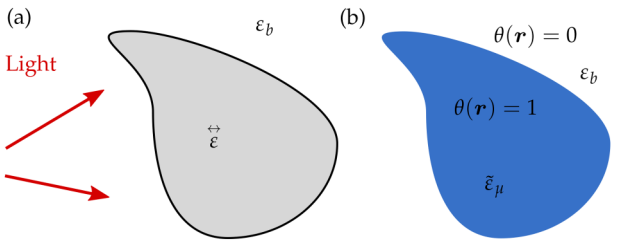

FIG. 1. (a) Target system, an inclusion of arbitrary shape made of an anisotropic material, extending infinitely out of the plane. The dielectric function is noted $\overleftrightarrow{\varepsilon}$. The background is an isotropic medium with permittivity ε_b. (b) Basis system, an isotropic inclusion with dielectric function $\tilde{\varepsilon}_\mu$ and same geometry as in (a) embedded in the same background. The function $\theta(\boldsymbol{r})$ is an indicator, which is 1 inside the inclusion (blue domain) and 0 outside (white domain).

free space Green's function, $\overleftrightarrow{G}_0(\boldsymbol{r}, \boldsymbol{r}')$, the vector Helmholtz equation can be converted to the Lippman–Schwinger equation,

$$\boldsymbol{E}(\boldsymbol{r}) = \boldsymbol{E}_0(\boldsymbol{r}) + k^2 \int_V \theta(\boldsymbol{r}')\overleftrightarrow{G}_0(\boldsymbol{r}, \boldsymbol{r}')\Delta\overleftrightarrow{\varepsilon}\, \boldsymbol{E}(\boldsymbol{r}')d\boldsymbol{r}', \quad (2)$$

where $\boldsymbol{E}_0(\boldsymbol{r}) = i\omega\mu_0 \int_V \overleftrightarrow{G}_0(\boldsymbol{r}, \boldsymbol{r}')\boldsymbol{J}(\boldsymbol{r}')d\boldsymbol{r}'$ is the incident electric field generated by the source of free current $\boldsymbol{J}(\boldsymbol{r})$. The second term on the right-hand-side of Eq. (2) corresponds to the scattered field generated by the polarization current.

Our aim is to construct a modal solution by defining a set of suitable modes to expand Eq. (2). To define an eigenvalue equation for modes of the anisotropic structure, $\boldsymbol{E}_m$, we shall use the source-free (i.e., $\boldsymbol{E}_0 = 0$) version of the Lippmann–Schwinger equation (2), namely,

$$s_m \boldsymbol{E}_m(\boldsymbol{r}) = k^2 \int_V \theta(\boldsymbol{r}')\overleftrightarrow{G}_0(\boldsymbol{r}, \boldsymbol{r}')\Delta\overleftrightarrow{\varepsilon}\boldsymbol{E}_m(\boldsymbol{r}')d\boldsymbol{r}', \quad (3)$$

where s_m is the associated eigenvalue. We shall call these modes, $\boldsymbol{E}_m$, the target modes. Use of these modes is greatly expedited if they obey an orthonormality relation. This exists for isotropic materials, since the integral operator defined in Eq. (3) is symmetric because $\overleftrightarrow{G}_0$ commutes with $\Delta\varepsilon\, \overleftrightarrow{I}$. For an isotropic inclusion of the same shape, Eq. (3) can be reduced to the definition $\tilde{s}_\mu \tilde{\boldsymbol{E}}_\mu = k^2 \int \theta(\boldsymbol{r}')G_0(\boldsymbol{r}, \boldsymbol{r}')\tilde{\boldsymbol{E}}_\mu(\boldsymbol{r}')d\boldsymbol{r}'$, where we have used $\tilde{\boldsymbol{E}}_\mu$ to denote these isotropic modes. They form a complete orthonormal basis of modes[32] for the bracket $\langle \tilde{E}_\mu | \tilde{E}_\nu \rangle = \int \theta(\boldsymbol{r})\tilde{\boldsymbol{E}}_\mu^\dagger(\boldsymbol{r}) \cdot \tilde{\boldsymbol{E}}_\nu(\boldsymbol{r})d\boldsymbol{r}$. Despite the similarity, this is not an "inner product" on a Hilbert space, because it lacks conjugate symmetry and is not positive definite. However, these conditions are not necessary for defining an orthogonality relationship useful for projection. More formally, this bracket defines a symmetric bilinear form, but we shall simply refer to it as "overlap integral" for the remainder of the paper.

For anisotropic materials however, we must establish an alternative orthonormality relation. Green's function $\overleftrightarrow{G}_0(\boldsymbol{r}, \boldsymbol{r}')$ does not commute, in general, with the permittivity contrast $\Delta\overleftrightarrow{\varepsilon}$, causing the integral operator (2) to be non-symmetric. Consequently, the target modes $\boldsymbol{E}_m$ do not form an orthogonal basis of modes under the above overlap integral. We develop the appropriate alternative in

Published under license by AIP Publishing.

Appendix A: $\langle E_m|\hat{\Theta}_\varepsilon|E_n\rangle = \int \theta(\boldsymbol{r})\boldsymbol{E}_m^\dagger(\boldsymbol{r})\cdot\Delta\overleftrightarrow{\varepsilon}\boldsymbol{E}_n(\boldsymbol{r})d\boldsymbol{r}$, where the operator Θ_ε emphasizes the presence of the permittivity contrast $\Delta\overleftrightarrow{\varepsilon}$. The derivation of this new overlap integral imposes a condition on the types of $\Delta\overleftrightarrow{\varepsilon}$ that we may treat: the matrix square root of permittivity tensor must be complex symmetric. This condition is simple to verify numerically. In some cases, it can be formally proven to be true, such as for materials with orthogonal principal axes, whether lossless or lossy. Further details are provided in Appendix B. The target modes now form a complete set of orthogonal modes and can be used to solve the Lippmann–Schwinger equation for the total fields over all space using

$$\boldsymbol{E}(\boldsymbol{r}) = \boldsymbol{E}_0(\boldsymbol{r}) + \sum_m \boldsymbol{E}_m(\boldsymbol{r})\frac{s_m}{1-s_m}\langle E_m|\hat{\Theta}_\varepsilon|E_0\rangle, \tag{4}$$

also derived in Appendix A.

However, one challenging task remains: finding the target modes by solving either the integral or differential equation that they satisfy. To overcome this issue, we re-expand the target modes in terms of modes of an isotropic inclusion of the same shape.[42] We shall call the modes of the latter the basis modes, defined above as $\tilde{\boldsymbol{E}}_\mu(\boldsymbol{r})$. We expand $\boldsymbol{E}_m(\boldsymbol{r}) = \sum_\mu c_{\mu,m}\tilde{\boldsymbol{E}}_\mu(\boldsymbol{r})$, where the coefficients $c_{\mu,m}$ can be found by solving the linear eigenvalue problem derived in Appendix A,

$$s_m\boldsymbol{c}_m = S\,V\boldsymbol{c}_m. \tag{5}$$

Here, V is the matrix of overlap integral between the modes of the isotropic inclusion, $\langle\tilde{E}_\mu|\hat{\Theta}_\varepsilon|\tilde{E}_\nu\rangle$, and S is the diagonal matrix of eigenvalue $\tilde{s}_\mu$ of the modes of the isotropic inclusion. Equation (5) is key to understanding how the modes of an anisotropic inclusion differ from the modes of an isotropic inclusion. For an isotropic inclusion, one can easily verify that the overlap matrix V is diagonal due to the orthogonality relation of the basis modes. In that case, there is no coupling between the modes. The isotropic case allows us to interpret the eigenvalue $\tilde{s}_\mu$ in terms of eigenpermittivity $\tilde{\varepsilon}_\mu$ as

$$\tilde{s}_\mu = \frac{1}{\tilde{\varepsilon}_\mu - \varepsilon_b}. \tag{6}$$

Conversely, for anisotropic materials, the matrix of overlap integrals is not diagonal. Its off-diagonal terms result from the coupling between two different basis modes induced by the anisotropy. It is worth noting the coupling between basis modes with different symmetrical properties (e.g., symmetry forbidden in the isotropic case) may be allowed with anisotropic materials.

Furthermore, the anisotropy introduces a longitudinal component to the fields inside the inclusion. From Maxwell's equations, we have $\nabla\cdot\overleftrightarrow{\varepsilon}\boldsymbol{E} = 0$, so, in general, the electric field is not divergence-free, i.e., $\nabla\cdot\boldsymbol{E} \neq 0$. To ensure that the basis modes $\tilde{\boldsymbol{E}}_\mu(\boldsymbol{r})$ form a complete set and are able to account for the longitudinal component of the resulting electric fields $\boldsymbol{E}$, longitudinal basis modes must be considered, satisfying $\nabla\cdot\tilde{\boldsymbol{E}}_\mu \neq 0$ inside the inclusion. Such longitudinal modes always exist, even in isotropic inclusions, but are not excited by far-field sources, though they are excited by near-field sources inside the inclusion. They are associated with the eigenpermittivity $\tilde{\varepsilon}_\mu = 0$ and a complete set can be constructed using the cavity modes of an electrostatic resonator of the same shape.[42]

For practical applications, it is more convenient to compare the results from multiple simulations with different $\overleftrightarrow{\varepsilon}$ if Eq. (4) is re-written in terms of a common set of modes that have the same scattering patterns, i.e., the basis modes. In these terms, Eq. (4) becomes

$$\boldsymbol{E}(\boldsymbol{r}) = \boldsymbol{E}_0(\boldsymbol{r}) + \sum_\mu \gamma_\mu\tilde{\boldsymbol{E}}_\mu(\boldsymbol{r}), \tag{7}$$

where $\gamma_\mu = \sum_m c_{\mu,m}\frac{s_m}{1-s_m}\langle E_m|\hat{\Theta}_\varepsilon|E_0\rangle$.

III. NUMERICAL SIMULATIONS OF HYPERBOLIC ANISOTROPIC INFINITE CYLINDER

A. Physical configuration

The procedure for treating anisotropic cylinders with arbitrary cross sections is first to find the modes of the isotropic inclusion. Examples for arbitrary cross section with isotropic materials can be found in Refs. 32 and 45 using commercial finite element software to compute the modes, and in Ref. 51 with a re-expansion approach. In the following, to exemplify our re-expansion approach for anisotropic materials, we consider a fairly simple geometry for which the modes of the isotropic equivalent are available analytically. We consider an infinitely long cylinder exhibiting hyperbolic behavior.

Hyperbolic metamaterials are characterized by complex permittivity tensors and are studied for their unusual optical properties. The patterning and nanostructuring of these materials is of great interest for realizing new types of optical functions.[52,53] The dispersion relation in such a material is given by

$$\frac{k_{\phi,z}^2}{\varepsilon_\rho} + \frac{k_\rho^2}{\varepsilon_{\phi,z}} = k_0^2, \tag{8}$$

where $k_{\phi,z}$ and k_ρ are the in-plane and out-of-plane components of the wavevector in the cylinder and the real part of the in-plane and out-of-plane components of the permittivity tensor have opposite signs, $Re(\varepsilon_{\phi,z})Re(\varepsilon_\rho) < 0$. The domain where $Re(\varepsilon_{\phi,z}) > 0$ is called type I and the domain where $Re(\varepsilon_{\phi,z}) < 0$ is called type II.[53]

In what follows, we shall consider an infinite cylinder along the z-axis with a circular cross section in the (x, y)-plane [Fig. 2(a)] of radius $R = 90$ nm. The cylindrical inclusion consists of concentric multilayers of silver[54] and titanium oxide[55] known to exhibit hyperbolic behavior in the visible range.[56] We denote the filling factor of silver in the composite by p. We assume that the layers are thin enough so that we can apply effective medium theory,[8] resulting in a homogeneous uniaxial anisotropic system described in the cylindrical coordinate system,

$$\overleftrightarrow{\varepsilon} = \begin{pmatrix} \varepsilon_\rho & 0 & 0 \\ 0 & \varepsilon_{\phi,z} & 0 \\ 0 & 0 & \varepsilon_{\phi,z} \end{pmatrix}_{(\hat{\boldsymbol{e}}_\rho,\hat{\boldsymbol{e}}_\phi,\hat{\boldsymbol{e}}_z)}, \tag{9}$$

Published under license by AIP Publishing.

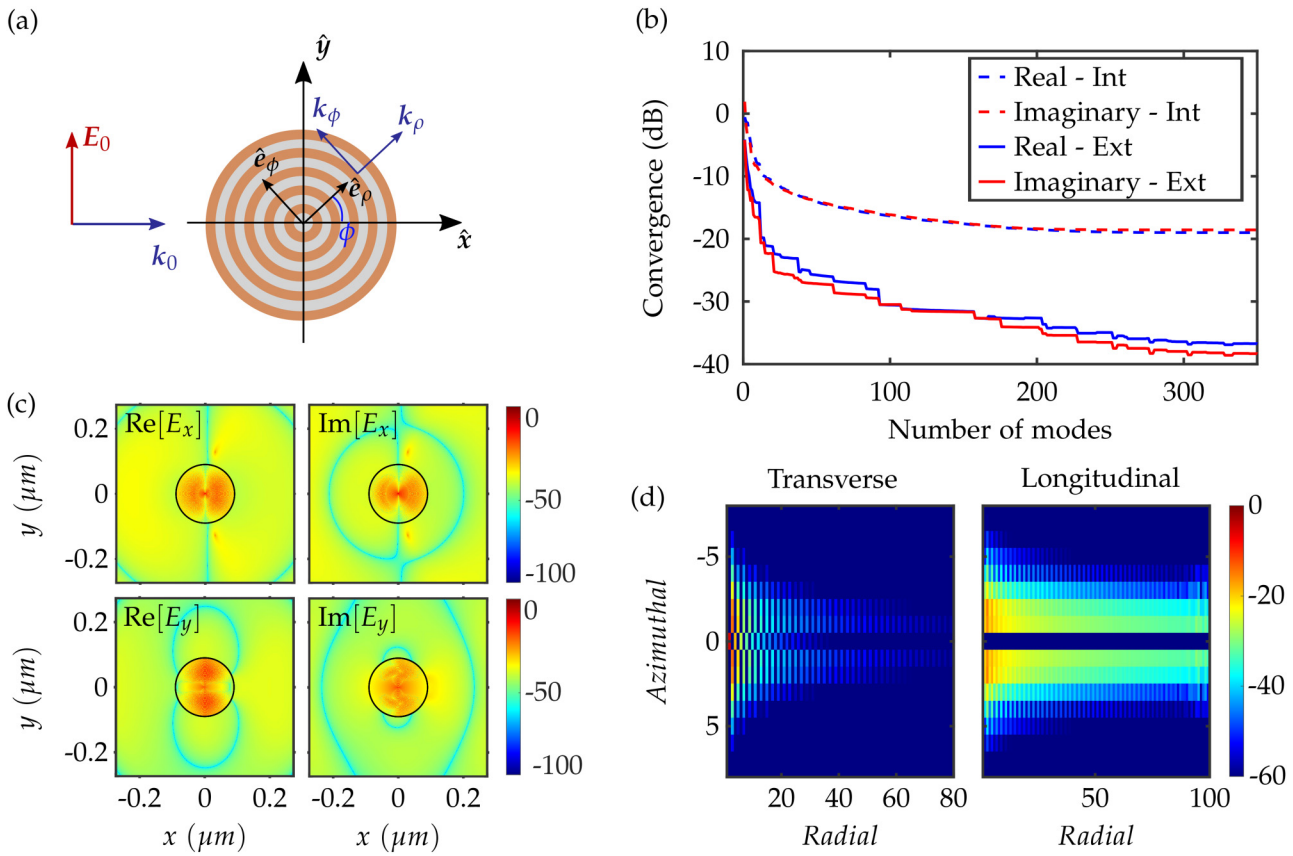

FIG. 2. (a) Schematic of the concentric layered scatterer. A plane wave that is linearly polarized and transverse magnetic is propagating along the $\hat{\boldsymbol{x}}$. (b) Convergence of the total electric field between Mie and GENOME solutions. The dashed line represents the agreement inside the cylinder and the solid line the agreement outside. (c) Difference, in dB, between the electric fields computed with Mie and GENOME solutions. (d) Map of the coefficient $|\gamma_n|$, Eq. (7), normalized by the largest coefficient, in dB. At 470 nm, the permittivity contrasts are $\varepsilon_\rho = -16.32 + 3.15i$ and $\varepsilon_{\phi,z} = -2.65 + 0.49i$.

where

$$\varepsilon_{\phi,z} = p\varepsilon_{\mathrm{Ag}} + (1-p)\varepsilon_{\mathrm{TiO_2}}, \quad \varepsilon_\rho = \frac{1}{\frac{p}{\varepsilon_{\mathrm{Ag}}} + \frac{1-p}{\varepsilon_{\mathrm{TiO_2}}}}. \tag{10}$$

Here, we emphasize that (a) we do not consider the material to be lossless, so the permittivities of the titanium oxide ε_{TiO_2} and silver ε_{Ag} are complex; (b) we may treat media of any material dispersion relation, since we operate in the frequency domain and treat each frequency independently. We note also that the principal axes of the permittivity tensor form an orthogonal basis, so the condition of Appendix B on the material is satisfied. Additionally, we note the presence of a singularity in the dielectric function of Eq. (9) at the center of the cylinder ($\rho = 0$) when expressed with Cartesian unit vectors ($\hat{\boldsymbol{e}}_x$, $\hat{\boldsymbol{e}}_y$, $\hat{\boldsymbol{e}}_z$), since the permittivity tensor is constant in the cylindrical basis ($\hat{\boldsymbol{e}}_\rho$, $\hat{\boldsymbol{e}}_\phi$, $\hat{\boldsymbol{e}}_z$) where $\hat{\boldsymbol{e}}_\rho = \boldsymbol{\rho}/\rho$.

The illumination source is chosen to be a monochromatic plane wave propagating along the x-direction with $\boldsymbol{E}_0$ directed in the y-direction. The basis modes corresponding to the equivalent isotropic structure are determined analytically for the transverse modes[44] and the longitudinal modes.[42] The details of the derivation of the overlap integrals, $\langle E_m|\hat{\Theta}_\varepsilon|E_0\rangle$ in Eq. (7), between the modes and the incident field are presented in Appendixes C and D.

B. Validating the re-expansion approach with COMSOL

To validate our model, we have compared the electric field generated by GENOME (7) with the solution given by Mie theory.[49,50] The relative error between the Mie solution and GENOME (7) is evaluated using the L_2-norm,

$$\Delta\eta_R = \frac{\|\mathrm{Re}(\boldsymbol{E}_{\mathrm{Mie}} - \boldsymbol{E}_{\mathrm{GENOME}})\|_2}{\|\mathrm{Re}(\boldsymbol{E}_{\mathrm{Mie}})_2}, \tag{11}$$

$$\Delta\eta_I = \frac{\|\mathrm{Im}(\boldsymbol{E}_{\mathrm{Mie}} - \boldsymbol{E}_{\mathrm{GENOME}})\|_2}{\|\mathrm{Im}(\boldsymbol{E}_{\mathrm{Mie}})\|_2}. \tag{12}$$

Published under license by AIP Publishing.

For this test, we consider the operating wavelength 470 nm and $p = 0.7$. The solution is computed twice. We first compute with a large amount of modes, so as to find the most significant modes of the modal decomposition, and then with only the selected modes for comparisons.[57]

The convergence between Mie and our solutions is plotted in Fig. 2(b). Outside the cylinder, we observe respectable agreement between the two solutions, up to −36 dB. However, inside the cylinder, the convergence reaches only −18 dB. This difference can be seen in the field plot [Fig. 2(c)], where the difference is largest at the center of the cylinder, close to the singularity. Further convergence is impeded by the truncation of high radial order longitudinal modes, as shown in the map of the coefficient γ_n [Fig. 2(d)]. The decay in the magnitudes of γ_n with progressively higher radial order is slower for the longitudinal modes than for the transverse modes.[58] The main issue in the convergence should be resolved by using a more realistic geometry with an isotropic core, thus removing the singularity but introducing a discontinuity.

C. Application to hyperbolic metamaterials

We now use our method to study the scattering properties of a hyperbolic metamaterial cylinder with a radially anisotropic permittivity tensor. These structures have received much attention recently for realizing superscattering.[59,60] In our example, the diameter of the cylinder is 180 nm and we shall tune the composition of silver (p) in the material.

To describe the modes, we adopt the convention for the modes of an optical fiber. Therefore, the modes are transverse electric TE since the electric field is confined to the plane perpendicular to the axis of the cylinder. The superscripts d and p indicate whether the mode is dielectric or plasmonic, corresponding to a positive or negative real part of the eigenpermittivity (6), respectively, and the subscript denotes the azimuthal order of the mode. A visual representation of the modes TE_0^d, TE_1^d, TE_1^p, TE_2^d, and TE_2^p is provided in Fig. 3. These modes can be associated with the excitation of magnetic or electric multi-poles. Plasmonic modes, defined by $Re(\tilde{\varepsilon}_\mu) < 0$, are associated with electric fields that do not oscillate radially in the cylinder. In our case, they can be associated to the excitation of electric dipoles, TE_1^p and electric quadrupole, TE_2^p . Conversely, dielectric modes are defined by $Re(\tilde{\varepsilon}_\mu) > 0$ have their fields oscillate inside the cylinder. In our case, TE_1^d and TE_2^d are, respectively, a magnetic dipole and quadrupole since the internal electric field induce pairs of current loops (respectively, 1 and 2 pairs) with opposite circulation.

In Fig. 4, we first present the modal analysis for a purely isotropic cylinder. In the case of a purely dielectric cylinder ($p = 0$) [Fig. 4(a)], we observe three scattering peaks, at 360 nm, 420 nm,

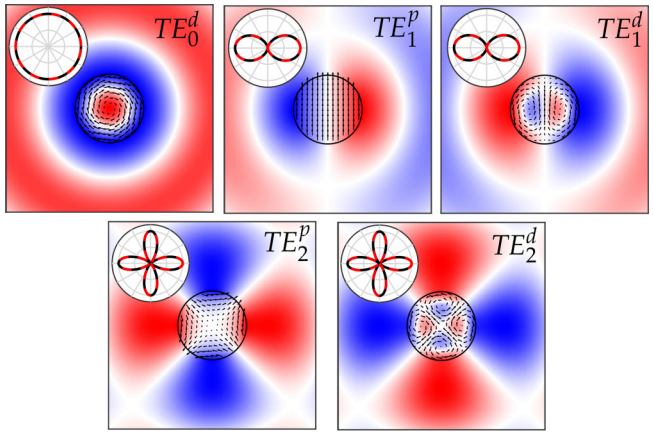

FIG. 3. Magnetic fields of the basis modes. The electric field inside the cylinder is represented by black arrows. The far-field intensities of the electric (black plain) and magnetic (red dashed) fields are represented in the radar plots in the insets of each panel.

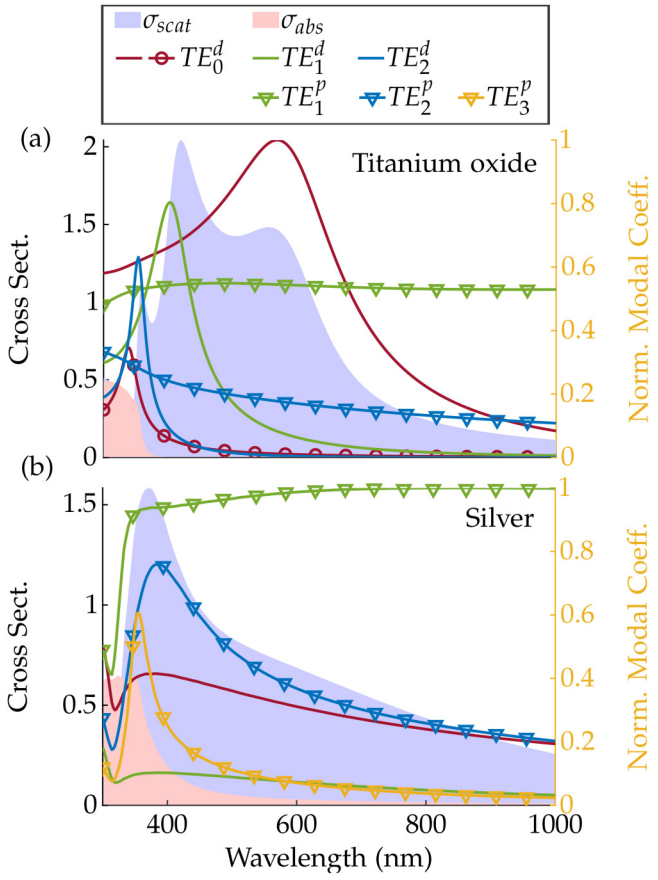

FIG. 4. Cylinder with diameter 180 nm for isotropic materials: (a) titanium oxide and (b) silver. The blue and red areas represent the scattering and absorption cross sections, respectively, and are associated with the left y axis. The cross sections have been normalized by the diameter of the cylinder. The curves represent the coefficient $|\gamma_n|$, Eq. (7), for the most important modes. The coefficients have been normalized by the maximum of the most important modes.

Published under license by AIP Publishing.

and 560 nm, which correspond to the resonances of three dielectric modes. We note also that scattering behavior of the cylinder is dominated by the electric dipole TE_1^p. For the pure silver cylinder ($p = 1$) [Fig. 4(b)], we observe only one scattering resonance at 370 nm corresponding to the superposition of several higher order modes that are resonant around the same wavelength. Since the material is metallic, the incidence field is not strongly coupled to the dielectric modes.

We now consider the modal decomposition of the scattered field for a hyperbolic cylinder with a composition of $p = 0.4$, displayed in Fig. 5. In the first panel, we plot the in-plane and out-of-plane permittivities (10), which are characteristic to this type of composite material with the presence of epsilon-near-pole and epsilon-near-zeros. Both type I and type II hyperbolic media are present. On the second and third panels, we plot only the most significant basis modes of the decomposition of the scattered field (7), other modes being negligible. The longitudinal modes are denoted as L with the azimuthal order as the subscript. Inspecting the second panel and the scattering spectrum, we may observe several scattering peaks. Two of them, at 356 nm and 390 nm, are in the type I domain. From the modal analysis, we can see that the material acts mainly as a dielectric in the type I domain since dielectric modes dominate the scattering response of the cylinder. Conversely, in the type II domain, the amplitudes of the dielectric modes drop considerably and the plasmonic modes become predominant, which confers the metallic character of the type II hyperbolic metamaterials. In the second panel, we also observe two dips in the scattering cross section, at 550 nm and 850 nm. These dips correspond to the coupling between the plasmonic modes and the longitudinal modes. The longitudinal modes, being confined within the cylinder, do not contribute to the scattering. However, resonances of the longitudinal components contribute to the generation of absorption peaks.

Additionally, by tuning the filling factor, p, of the material we can further control the spectral positions of scattering and

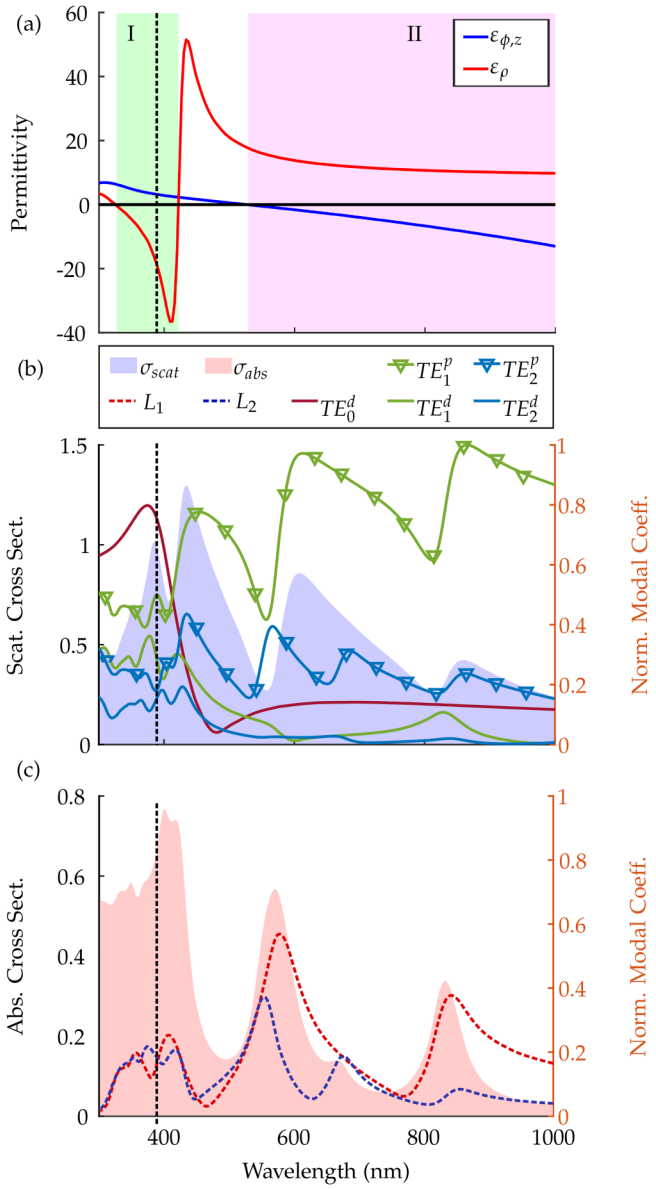

FIG. 5. Cylinder with diameter 180 nm and material with composition of silver $p = 0.4$. (a) Real part of the in-plane (red) and out-of-plane (blue) components of the effective permittivity tensor. The green and purple domains show the domains in which the material is hyperbolic type I or II, respectively. (b) Scattering cross section (blue area), corresponding to the left axis. The evolution of the coefficient γ_μ is represented by the curve respectively to the right axis. Only the transverse modes have been plotted. (c) Absorption cross section (red area) and coefficients of longitudinal modes (dashed lines). The coefficients $|\gamma_n|$ have been normalized by the most important mode.

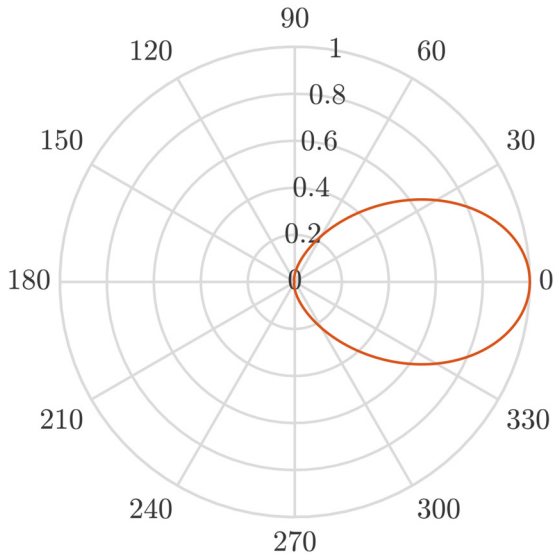

FIG. 6. Far-field pattern of the field scattered by the anisotropic cylinder with diameter 180 nm at a wavelength 389 nm and for a composition of silver $p = 0.4$ shown in Fig. 5 by the dashed line.

Published under license by AIP Publishing.

absorption.[61] Moreover, the design flexibility provided by the controllable effective index of the hyperbolic response allows us to adjust the nanostructure scattering diagram at will. For example, we see in Fig. 6 that within the type I domain, there is suppression of the backscattering due to the constructive and destructive interferences of the excited modes. This is also known as Kerker effect.[62] Our modal decomposition reveals that the superposition of four modes (electric dipole TE_1^p, an electric quadrupole TE_2^p, a magnetic dipole TE_1^d and a magnetic quadrupole TE_2^d) with the correct phase condition can suppress both backward scattering and the sidelobes.[63]

IV. OUTLOOK

In this paper, we presented an extension of GENOME to anisotropic materials. We solved the challenges that stem from anisotropy—namely, the loss of symmetry of the scattering operator and the difficulty of computing the modes— by re-expanding the electric fields in terms of modes of the equivalent isotropic inclusion. We illustrated our method by comparing to the Mie solution and achieved reasonable agreement. However, our modal expansion is applicable to arbitrary geometries as well as dissipative systems[51] and provides a comprehensive modal decomposition of the scattered field. We applied the decomposition to study the scattering by a cylinder with hyperbolic concentric layers to yield insight into its scattering properties such as the absorption process and the cancellation of backscattering in a type I hyperbolic medium.

Our re-expansion method applied to anisotropic materials can already be used for a number of subsequent applications where the modes of the isotropic inclusion are already known, which paves the way for new developments in nanophotonics such as the design of new superscatterers or enhancement of spontaneous emission.

ACKNOWLEDGMENTS

P.Y.C. and Y.S. were partially supported by Israel Science Foundation (ISF) (Grant No. 899/16). N.K. and Q.J.W. were partially supported by the Singapore Ministry of Education (Grant No. MOE2018-T2-1-176), Advanced Manufacturing and Engineering Grant from the Agency for Science, Technology and Research (A*STAR) (Award No. A18A7b0058). P.G. was partially supported by the European Research Council (ERC Grant No. 639109). N.K. thanks Assistant Professor Luo Yu (Nanyang Technological University) for the insightful discussions related to hyperbolic metamaterials.

APPENDIX A: GENERALIZED NORMAL MODES EXPANSION FOR ANISOTROPIC SCATTERERS

1. Lippman–Schwinger equation and symmetrization

Let us consider an infinitely long inclusion with an anisotropic homogeneous permittivity tensor $\overleftrightarrow{\varepsilon}$ embedded in an isotropic homogeneous background medium of permittivity ε_b (Fig. 1). We define $\Delta\overleftrightarrow{\varepsilon} \equiv \overleftrightarrow{\varepsilon} - \varepsilon_b$ to be the difference between the inclusion and the background permittivities.

For monochromatic wave illumination, Maxwell's equations lead to the wave equation inside the inclusion,

$$\nabla \times \nabla \times \boldsymbol{E}(\boldsymbol{r}) - k^2 \overleftrightarrow{\varepsilon}\, \boldsymbol{E}(\boldsymbol{r}) = i\omega\mu_0 \boldsymbol{J}(\boldsymbol{r}), \tag{A1}$$

and outside,

$$\nabla \times \nabla \times \boldsymbol{E}(\boldsymbol{r}) - k^2 \varepsilon_b\, \boldsymbol{E}(\boldsymbol{r}) = i\omega\mu_0 \boldsymbol{J}(\boldsymbol{r}), \tag{A2}$$

with $k = \omega c$ being the wavevector in free space, ω the frequency, μ_0 the free space permeability, $\boldsymbol{J}$ the free current, and employing $e^{i\omega t}$ time harmonic variation throughout. Subtracting the term $k^2\varepsilon_b\boldsymbol{E}$ from both sides of Eq. (A1), we introduce the indicator function $\theta(\boldsymbol{r})$ that is 1 inside the inclusion and 0 outside [see Fig. 1(b)] so that we can combine Eqs. (A1) and (A2) into

$$\nabla \times \nabla \times \boldsymbol{E}(\boldsymbol{r}) - k^2\varepsilon_b \boldsymbol{E}(\boldsymbol{r}) = i\omega\mu_0 \boldsymbol{J}(\boldsymbol{r}) + k^2\theta(\boldsymbol{r})\,\Delta\overleftrightarrow{\varepsilon}\, \boldsymbol{E}(\boldsymbol{r}), \tag{A3}$$

which is valid everywhere. In Eq. (A3), we treat the inclusion as a source term induced by the permittivity contrast, which is equivalent to the polarization current. The free space Green's tensor $\overleftrightarrow{G}_0(\boldsymbol{r}, \boldsymbol{r}')$ associated with the left-hand side of Eq. (A3) is the solution of[64]

$$\nabla \times \nabla \times \overleftrightarrow{G}_0(\boldsymbol{r}, \boldsymbol{r}') - k^2\varepsilon_b \overleftrightarrow{G}_0(\boldsymbol{r}, \boldsymbol{r}') = \overleftrightarrow{I}\,\delta(\boldsymbol{r} - \boldsymbol{r}'), \tag{A4}$$

where $\overleftrightarrow{I}$ is the identity matrix. The free space Green's tensor can be used to write down a formal solution of Eq. (A3) as

$$\begin{aligned} \boldsymbol{E}(\boldsymbol{r}) &= \boldsymbol{E}_0(\boldsymbol{r}) + \hat{\Gamma}\hat{\Theta}_\varepsilon \boldsymbol{E}(\boldsymbol{r}), \\ \hat{\Gamma}\Theta_\varepsilon \boldsymbol{E}(\boldsymbol{r}) &\equiv k^2 \int_V \theta(\boldsymbol{r}')\overleftrightarrow{G}_0(\boldsymbol{r}, \boldsymbol{r}')\Delta\overleftrightarrow{\varepsilon}\, \boldsymbol{E}(\boldsymbol{r}')d\boldsymbol{r}', \end{aligned} \tag{A5}$$

which is the Lippman–Schwinger equation for electromagnetism. It was obtained by convolving the free-space Green's tensor with the two terms on the right-hand-side of Eq. (A3). The first one

$$\boldsymbol{E}_0(\boldsymbol{r}) = i\omega\mu_0 \int_V \overleftrightarrow{G}_0(\boldsymbol{r}, \boldsymbol{r}')\boldsymbol{J}(\boldsymbol{r}')d\boldsymbol{r}'. \tag{A6}$$

corresponds to the incident field generated by the source of free current $\boldsymbol{J}$ while the second term is the scattered field generated by the polarization current. In the case of an isotropic inclusion, the permittivity tensor is a scalar multiple of the identity matrix, $\Delta\overleftrightarrow{\varepsilon} = \Delta\varepsilon\overleftrightarrow{I}$. Then, the permittivity in Eq. (A5) can be factorized out of the integral and the new operator becomes

$$\hat{\Gamma}\boldsymbol{E}(\boldsymbol{r}) = k^2\Delta\varepsilon \int_V \theta(\boldsymbol{r}')\,\overleftrightarrow{G}_0(\boldsymbol{r}, \boldsymbol{r}')\boldsymbol{E}(\boldsymbol{r}')d\boldsymbol{r}'. \tag{A7}$$

Here, we can make two observations. First, the linear operator $\hat{\Gamma}$ is symmetric under matrix transposition,[32] and thus defines a set of orthogonal eigenmodes under the overlap integral

$$\int_V \theta(\boldsymbol{r})\tilde{\boldsymbol{E}}_\nu^\dagger(\boldsymbol{r})\tilde{\boldsymbol{E}}_\mu(\boldsymbol{r})d\boldsymbol{r} = \delta_{\mu,\nu}, \tag{A8}$$

where the superscript † denotes the adjoint mode and implies transposition without complex conjugation. Second, Eq. (A7) is

Published under license by AIP Publishing.

written in its integral form but the differential form is also known: it is the source-free Helmholtz equation,

$$\nabla \times \nabla \times \boldsymbol{E}(\boldsymbol{r}) - k^2 \varepsilon_b \boldsymbol{E}(\boldsymbol{r}) = k^2 \theta(\boldsymbol{r}) \Delta\varepsilon \boldsymbol{E}(\boldsymbol{r}). \tag{A9}$$

The complication associated with anisotropic materials now becomes clear—the permittivity tensor and Green's tensors do not commute in general. Thus, the linear operator $\hat{\Gamma}\hat{\Theta}_\varepsilon$ defined in Eq. (A5) is non-symmetric, and its modes do not necessarily form an orthogonal basis according to the overlap integral (A8). From Eq. (A5), the modes E_m of the operator $\hat{\Gamma}\hat{\Theta}_\varepsilon$ are defined by

$$s_m \boldsymbol{E}_m = k^2 \int_V \theta(\boldsymbol{r}') \overleftrightarrow{G}_0(\boldsymbol{r}, \boldsymbol{r}') \Delta\overleftrightarrow{\varepsilon} \boldsymbol{E}_m(\boldsymbol{r}') d\boldsymbol{r}', \tag{A10}$$

where s_m is the eigenvalue.

To overcome this issue, we exploit the symmetry of the permittivity tensor[65] to symmetrize the operator $\hat{\Gamma}\hat{\Theta}_\varepsilon$ and define a new overlap integral that yields an orthogonality relation for the modes $\boldsymbol{E}_m$. Specifically, we introduce the square root R of the permittivity tensor,[47] $\Delta\overleftrightarrow{\varepsilon} = RR$, and multiply Eq. (A10) by R from the left. This gives

$$s_m \overleftrightarrow{R} \boldsymbol{E}_m(\boldsymbol{r}) = k^2 \int_V \theta(\boldsymbol{r}') \overleftrightarrow{R}\, \overleftrightarrow{G}_0(\boldsymbol{r}, \boldsymbol{r}')\, \overleftrightarrow{R}\, \overleftrightarrow{R} \boldsymbol{E}_m(\boldsymbol{r}') d\boldsymbol{r}'. \tag{A11}$$

Introducing the temporary notation, $\boldsymbol{F} \equiv \overleftrightarrow{R}\boldsymbol{E}$, Eq. (A11) becomes

$$s_m \boldsymbol{F}_m(\boldsymbol{r}) = k^2 \int_V \theta(\boldsymbol{r}') \overleftrightarrow{R}\, \overleftrightarrow{G}_0(\boldsymbol{r}, \boldsymbol{r}')\, \overleftrightarrow{R}\, \boldsymbol{F}_m(\boldsymbol{r}') d\boldsymbol{r}'. \tag{A12}$$

The new operator $\overleftrightarrow{R}\, \overleftrightarrow{G}_0(\boldsymbol{r}, \boldsymbol{r}')\, \overleftrightarrow{R}$ in Eq. (A12) is symmetric under transposition so its right eigenmodes, $\boldsymbol{F}_m$, define a complex orthogonal basis for the overlap integral,

$$\int_V \theta(\boldsymbol{r}) \boldsymbol{F}_n^\dagger(\boldsymbol{r}) \boldsymbol{F}_m(\boldsymbol{r}) d\boldsymbol{r} = \delta_{nm}. \tag{A13}$$

Therefore, from this analysis, we deduce that the modes $\boldsymbol{E}_m$ of the operator $\hat{\Gamma}\hat{\Theta}_\varepsilon$ satisfy the orthogonality relation

$$\int_V \theta(\boldsymbol{r}) \boldsymbol{E}_n^\dagger(\boldsymbol{r}) \Delta\overleftrightarrow{\varepsilon} \boldsymbol{E}_m(\boldsymbol{r}) d\boldsymbol{r} = \delta_{nm}, \tag{A14}$$

which defines the overlap integral appropriate to our problem. Using the bracket notation, the overlap integral is denoted $\langle E_n | \hat{\Theta}_\varepsilon | E_m \rangle$, where $\hat{\Theta}_\varepsilon$ is the operator associated with the step function θ and the permittivity tensor $\Delta\overleftrightarrow{\varepsilon}$ and Eq. (A10) can be written as

$$s_m |E_m\rangle = \hat{\Gamma}\hat{\Theta}_\varepsilon |E_m\rangle. \tag{A15}$$

At this point, the differential form of Eq. (A15) remains unknown, and it is complicated to directly construct the set of orthogonal modes for anisotropic materials. In order to overcome this limitation, we show below how to use the known modes of an isotropic inclusion of the same shape to construct an orthonormal set of new modes using the re-expansion method.[42]

2. The re-expansion method

a. Derivation of the re-expansion eigenvalue problem

Let us consider an inclusion composed of material with an isotropic permittivity ε_μ and having the exact same shape as our anisotropic inclusion of interest. In the absence of free current sources, the vector Helmholtz equation for the isotropic case, Eq. (A3), becomes

$$\nabla \times \nabla \times \tilde{\boldsymbol{E}}_\mu(\boldsymbol{r}) - k^2 \varepsilon_b \tilde{\boldsymbol{E}}_\mu(\boldsymbol{r}) = \frac{1}{\tilde{s}_\mu} \theta(\boldsymbol{r}) k^2 \varepsilon_b \tilde{\boldsymbol{E}}_\mu(\boldsymbol{r}), \tag{A16}$$

where $\tilde{s}_\mu = \varepsilon_b/(\varepsilon_\mu - \varepsilon_b)$ is the Bergman spectral parameter[38] and corresponds to the eigenvalue associated with the mode $\tilde{\boldsymbol{E}}_\mu$.

Since $\tilde{\boldsymbol{E}}_\mu$ forms a complete set inside the inclusion,[32] we decompose the modes of the anisotropic inclusion,[42] also called the target modes, in terms of modes of the isotropic inclusion

$$\boldsymbol{E}_m(\boldsymbol{r}) = \sum_\mu c_{\mu,m} \tilde{\boldsymbol{E}}_\mu(\boldsymbol{r}). \tag{A17}$$

These modes satisfy

$$\nabla \times \nabla \times \boldsymbol{E}_m(\boldsymbol{r}) - k^2 \varepsilon_b \boldsymbol{E}_m(\boldsymbol{r}) = \frac{1}{s_m} \theta(\boldsymbol{r}) k^2 \Delta\overleftrightarrow{\varepsilon} \boldsymbol{E}_m(\boldsymbol{r}). \tag{A18}$$

Inserting the decomposition of the target modes (A17) in Eq. (A18) yields

$$\sum_\mu c_{\mu,m} \left[\nabla \times \nabla \times \tilde{\boldsymbol{E}}_\mu(\boldsymbol{r}) - k^2 \varepsilon_b \tilde{\boldsymbol{E}}_\mu(\boldsymbol{r})\right] = \frac{1}{s_m} \theta(\boldsymbol{r}) k^2 \Delta\overleftrightarrow{\varepsilon} \sum_\mu c_{\mu,m} \tilde{\boldsymbol{E}}_\mu(\boldsymbol{r}). \tag{A19}$$

We replace the terms in the brackets on the left-hand side of Eq. (A19) by the right-hand-side of Eq. (A16). This leads to

$$\sum_\mu c_{\mu,m} \frac{1}{\tilde{s}_\mu} \theta(\boldsymbol{r}) k^2 \varepsilon_b \tilde{\boldsymbol{E}}_\mu(\boldsymbol{r}) = \frac{1}{s_m} \theta(\boldsymbol{r}) k^2 \Delta\overleftrightarrow{\varepsilon} \sum_\mu c_{\mu,m} \tilde{\boldsymbol{E}}_\mu(\boldsymbol{r}). \tag{A20}$$

Then, we project Eq. (A20) along one of the basis modes $\tilde{\boldsymbol{E}}_\nu^\dagger$ and use the orthogonality relationship Eq. (A8). This yields

$$c_{\nu,m} \frac{1}{\tilde{s}_\nu} \varepsilon_b = \frac{1}{s_m} \sum_\mu c_{\nu,m} \int_V \theta(\boldsymbol{r}) \tilde{\boldsymbol{E}}_\nu^\dagger(\boldsymbol{r}) \Delta\overleftrightarrow{\varepsilon} \tilde{\boldsymbol{E}}_\mu(\boldsymbol{r}) d\boldsymbol{r}. \tag{A21}$$

We recognize on the right-hand-side of Eq. (A21) the overlap integral between the modes $\tilde{\boldsymbol{E}}_\nu^\dagger$ and $\tilde{\boldsymbol{E}}_\mu$,

$$v_{\nu,\mu} = \int_V \theta(\boldsymbol{r}) \tilde{\boldsymbol{E}}_\nu^\dagger(\boldsymbol{r}) \Delta\overleftrightarrow{\varepsilon}\, \tilde{\boldsymbol{E}}_\mu(\boldsymbol{r}) d\boldsymbol{r}, \tag{A22}$$

which represents the mixing between the modes of the isotropic inclusion due to the anisotropy of the material.

Published under license by AIP Publishing.

We rewrite Eq. (A21) as

$$s_m c_{\nu,m} = \frac{\tilde{s}_\nu}{\varepsilon_b} \sum_m c_{\mu,m} v_{\nu,\mu}, \tag{A23}$$

which using matrix notation is

$$s_m \boldsymbol{c}_m = S V \boldsymbol{c}_m, \tag{A24}$$

with $S = 1/(\varepsilon_b) diag[\tilde{s}_\mu]$ and $V = [v_{\nu,\mu}]$, the overlap integral matrix.

b. The total electric field

Using the modes obtained, we now solve the Lippmann–Schwinger equation (2) for a given incident field. Using the bracket notation introduced in Subsection 1 of Appendix A, Eq. (A5) can be rewritten as

$$|E\rangle = |E_0\rangle + \hat{\Gamma}\hat{\Theta}_\varepsilon |E\rangle. \tag{A25}$$

By inverting this relation, we can express the field $|E\rangle$ as a function of the incident field, namely,

$$|E\rangle = \left(1 - \hat{\Gamma}\hat{\Theta}_\varepsilon\right)^{-1} |E_0\rangle. \tag{A26}$$

The set of eigenmodes $\boldsymbol{E}_m$ forms a complete orthonormal base inside the inclusion[32] for the overlap integral (A14); therefore, we can write the following identity:

$$\overleftrightarrow{I} = \sum_m |E_m\rangle\langle E_m| \hat{\Theta}_\varepsilon. \tag{A27}$$

By multiplying on the right by $|E\rangle$, we have inside the inclusion

$$|E\rangle = \sum_m |E_m\rangle \langle E_m| \hat{\Theta}_\varepsilon |E\rangle. \tag{A28}$$

We substitute the term $|E\rangle$ on the right-hand-side of Eq. (A28) by its expression (A26), so that

$$|E\rangle = \sum_m |E_m\rangle \left\langle E_m| \hat{\Theta}_\varepsilon (1 - \hat{\Gamma}\hat{\Theta}_\varepsilon)^{-1} |E_0\right\rangle. \tag{A29}$$

The operator in the bracket can be rearranged via

$$\begin{aligned} \hat{\Theta}_\varepsilon (1 - \hat{\Gamma}\hat{\Theta}_\varepsilon)^{-1} &= \left[(1 - \hat{\Gamma}\hat{\Theta}_\varepsilon)\hat{\Theta}_\varepsilon^{-1}\right]^{-1} \\ &= \left[\hat{\Theta}_\varepsilon^{-1}(1 - \hat{\Theta}_\varepsilon\hat{\Gamma})\right]^{-1} \\ &= (1 - \hat{\Theta}_\varepsilon\hat{\Gamma})^{-1}\hat{\Theta}_\varepsilon. \end{aligned} \tag{A30}$$

We then apply the operator $(1 - \hat{\Gamma}\hat{\Theta}_\varepsilon)^{-1}$ to the adjoint $\langle E_m|$ so that inside the inclusion we have

$$|E\rangle = \sum_m |E_m\rangle \frac{1}{1 - s_m} \langle E_m| \hat{\Theta}_\varepsilon |E_0\rangle, \tag{A31}$$

whereas in order to get the field in all space, we insert (A31) into (A25) such that

$$|E\rangle = |E_0\rangle + \sum_m |E_m\rangle \frac{s_m}{1 - s_m} \langle E_m| \hat{\Theta}_\varepsilon |E_0\rangle. \tag{A32}$$

Equation (A32) gives the modal decomposition of the total field in terms of the target modes $|E_m\rangle$, with the scattered field represented by the sum over modes. The coefficients of this decomposition are expressed by the product of the detuning factor, $s_m/(1 - s_m)$[32] and the projection $\langle E_m|\hat{\Theta}_\varepsilon|E_0\rangle$, which represents the excitation of each mode by the incident source.

c. Orthogonality and adjoint modes

For geometries with degenerate modes, the relationship between the adjoint modes and direct modes is more intricate. A more detailed discussion can be found in Ref. 42. Here, we recall the main findings. The adjoint of the modes of the isotropic inclusion can be found by applying the following transformation:

$$\tilde{\boldsymbol{E}}_\mu^\dagger(r, \phi, z) = \tilde{\boldsymbol{E}}_\mu(r, -\phi, -z). \tag{A33}$$

Therefore, to fully determine the adjoint of the target modes, we must express the coefficients $b_{\mu,m}$ of the linear decomposition of the adjoint mode in the basis of modes of the isotropic inclusion

$$\boldsymbol{E}_m^\dagger(\boldsymbol{r}) = \sum_\mu b_{\mu,m} \tilde{\boldsymbol{E}}_\mu^\dagger(\boldsymbol{r}). \tag{A34}$$

The coefficient $b_{\mu,m}$ are unknown and to find how they are related to the coefficient $c_{\mu,m}$, one can derive, similarly to Subsection 2 of Appendix A, an equivalent relation to Eq. (A24) for the adjoint mode,

$$s_m \boldsymbol{b}_m = \boldsymbol{b}_m V S. \tag{A35}$$

The overlap integral matrix and the matrix of eigenvalue of isotropic inclusion do not commute, in general, which means that the linear coefficients of the adjoint mode decomposition are not the left eigenvectors of Eq. (A24). However, by writing the modes in a base of $(\cos m\theta, \sin m\theta)$ instead of the exponential base $(e^{im\theta}, e^{-im\theta})$, it is possible to solve Eqs. (A24) and (A35) at the same time since $V = V^T$.

APPENDIX B: CONDITIONS ON THE MATERIALS

We now consider the restrictions imposed by the assumptions in Appendix A 1 on the anisotropic permittivity tensors that may be treated in our formulation. We introduced the square root of the permittivity tensor $\overleftrightarrow{R}$ in order to define the overlap integral (A14). For our method to be applicable, this square root $\overleftrightarrow{R}$ must exist and be complex symmetric.

Many types of reciprocal media satisfy this requirement, and it is easily verified numerically. We do not exhaustively enumerate every type of medium which satisfies this requirement, but we prove that one type always does: biaxial anisotropic materials with orthogonal principal axis. For such materials, the permittivity

Published under license by AIP Publishing.

tensor can be diagonalized by a series of rotations, i.e.,

$$\Delta\overleftrightarrow{\varepsilon} = \overleftrightarrow{P}^{-1}\overleftrightarrow{D}\overleftrightarrow{P}, \quad \overleftrightarrow{P}^{-1} = \overleftrightarrow{P}^{T}. \tag{B1}$$

In this case, the square root $\overleftrightarrow{R}$ is given by $\overleftrightarrow{R} = \overleftrightarrow{P}^{T}\overleftrightarrow{D}^{\frac{1}{2}}\overleftrightarrow{P}$; clearly, $\overleftrightarrow{R}$ is symmetric.

Furthermore, for non-reciprocal materials, the permittivity tensor is not symmetric.[66] For example, with magneto-optic materials, also called gyrotropic materials, when there is no loss the permittivity tensor is complex and Hermitian.[67] More precisely, the off-diagonal terms of the permittivity tensor are pure imaginary with opposing signs, $\varepsilon_{xy} = -\varepsilon_{yx} = i\varepsilon_g$.[68] Thus, the permittivity tensor satisfies Eq. (B1) with instead $\overleftrightarrow{P}^{-1} = \overleftrightarrow{P}^{*,T}$. Therefore, the square roots of the permittivity tensor are Hermitian, so not symmetric. We emphasize that there is no restriction on the imaginary part of the permittivity tensor so that scattering properties of lossy materials can be studied.

APPENDIX C: OVERLAP INTEGRALS

The overlap integral between the modes is calculated via

$$\nu_{\nu,\tau} = \int_V \theta(\boldsymbol{r})\tilde{\boldsymbol{E}}_\nu^\dagger(\boldsymbol{r}) \cdot \Delta\overleftrightarrow{\varepsilon}\tilde{\boldsymbol{E}}_\tau(\boldsymbol{r})d\boldsymbol{r}. \tag{C1}$$

So, the integrand in the right-hand-side of (C1) is a dot product of two vectors $\tilde{\boldsymbol{E}}_\nu^\dagger$ and $\Delta\overleftrightarrow{\varepsilon}\tilde{\boldsymbol{E}}_\tau$ that are expressed in the cylindrical base. However, for the following derivation, it is easier to express them in the rotational basis,

$$\hat{\boldsymbol{e}}_+ = \frac{1}{\sqrt{2}}(e^{i\phi}\hat{\boldsymbol{e}}_\rho + ie^{i\phi}\hat{\boldsymbol{e}}_\phi), \quad \hat{\boldsymbol{e}}_- = \frac{1}{\sqrt{2}}(e^{-i\phi}\hat{\boldsymbol{e}}_\rho - ie^{-i\phi}\hat{\boldsymbol{e}}_\phi). \tag{C2}$$

1. Transverse modes

From Ref. 44, we express the m-modes of the electric field inside the cylinder in a cylindrical base,

$$E_r = \left[C_\tau^E \frac{i\beta}{\alpha_\tau} J_\tau'(\alpha_\tau r) - C_\tau^H \frac{\tau k\mu}{r\alpha_\tau^2} J_\tau(\alpha_\tau r)\right] e^{i\tau\phi}e^{i\beta z}, \tag{C3}$$

$$E_\phi = \left[-C_\tau^E \frac{\tau\beta}{r\alpha_\tau^2} J_\tau(\alpha_\tau r) - C_\tau^H \frac{ik\mu}{\alpha_\tau} J_\tau'(\alpha_\tau r)\right] e^{i\tau\phi}e^{i\beta z}, \tag{C4}$$

$$E_z = C_\tau^E J_\tau(\alpha_\tau r)e^{i\tau\phi}e^{i\beta z}. \tag{C5}$$

To express this mode in the rotational basis, we project $\Delta\overleftrightarrow{\varepsilon}\tilde{\boldsymbol{E}}_\tau$ onto $\hat{\boldsymbol{e}}_+$ yielding

$$\tilde{E}_\tau^+ = \left[\frac{(\varepsilon_\rho - \varepsilon_{\phi,z})}{2} C_\tau^- J_{\tau-1}(\alpha_\tau r) + \frac{(\varepsilon_\rho + \varepsilon_{\phi,z})}{2} C_\tau^+ J_{\tau+1}(\alpha_\tau r)\right] \times e^{i(\tau+1)\phi}e^{i\beta z}, \tag{C6}$$

where we have defined the coefficient,

$$C_\tau^- = \frac{1}{\alpha_\tau\sqrt{2}}(i\beta C_\tau^E - k\mu C_\tau^H), \tag{C7}$$

$$C_\tau^+ = -\frac{1}{\alpha_\tau\sqrt{2}}(i\beta C_\tau^E + k\mu C_\tau^H). \tag{C8}$$

In a similar way, we project the $\Delta\overleftrightarrow{\varepsilon}\tilde{\boldsymbol{E}}_\tau$ onto $\hat{\boldsymbol{e}}_-$ and we obtain

$$\tilde{E}_\tau^- = \left[\frac{(\varepsilon_\rho + \varepsilon_{\phi,z})}{2} C_\tau^- J_{\tau-1}(\alpha_\tau r) + \frac{(\varepsilon_\rho - \varepsilon_{\phi,z})}{2} C_\tau^+ J_{\tau+1}(\alpha_\tau r)\right] \times e^{i(\tau-1)\phi}e^{i\beta z}. \tag{C9}$$

The adjoint form of the modes is written as[44]

$$\tilde{E}_\nu^\dagger = [C_\nu^E J_\nu(\alpha_\nu r)e^{-i\nu\phi}\hat{\boldsymbol{z}} + C_\nu^{\dagger,+} J_{\nu-1}(\alpha_\nu r)e^{-i(\nu-1)\phi}\hat{\boldsymbol{e}}_+ + C_\nu^{\dagger,-} J_{\nu+1}(\alpha_\nu r)e^{-i(\nu+1)\phi}\hat{\boldsymbol{e}}_-]e^{-i\beta z}, \tag{C10}$$

where

$$C_\nu^{\dagger,+} = -C_\nu^- \quad C_\nu^{\dagger,-} = -C_\nu^+. \tag{C11}$$

2. Longitudinal modes

The longitudinal modes are expressed[42] by

$$E_r = \frac{1}{2} L_{\tau\nu}\alpha_{\tau\nu}[J_{\tau-1}(\alpha_{\tau\nu}r) - J_{\tau+1}(\alpha_{\tau\nu}r)]e^{i\tau\phi}e^{i\beta z}, \tag{C12}$$

$$E_\phi = imL_{\tau\nu}\frac{J_\tau(\alpha_{\tau\nu}r)}{r}e^{i\tau\phi}e^{i\beta z}, \tag{C13}$$

$$E_z = i\beta L_{\tau\nu}J_\tau(\alpha_{\tau\nu}r)e^{i\tau\phi}e^{i\beta z}. \tag{C14}$$

So, in the rotational basis,

$$E_{\tau\nu}^+ = \left[\frac{(\varepsilon_\rho - \varepsilon_{\phi,z})}{2} D_{\tau\nu}^- J_{\tau-1}(\alpha_{\tau\nu}r)\frac{(\varepsilon_{\phi,z} + \varepsilon_\rho)}{2} D_{\tau\nu}^+ J_{\tau+1}(\alpha_{\tau\nu}r)\right] e^{i(\tau+1)\phi}e^{i\beta z}, \tag{C15}$$

where

$$D_{\tau\nu}^- = \frac{L_{\tau\nu}\alpha_{\tau\nu}}{\sqrt{2}}, \tag{C16}$$

$$D_{\tau\nu}^+ = -\frac{L_{\tau\nu}\alpha_{\tau\nu}}{\sqrt{2}}, \tag{C17}$$

Published under license by AIP Publishing.

and

$$E^{-}_{\tau\nu}=\left[\frac{(\varepsilon_{\phi,z}+\varepsilon_{\rho})}{2}D^{-}_{\tau\nu}J_{\tau-1}(\alpha_{\tau\nu}r)+\frac{(\varepsilon_{\rho}-\varepsilon_{\phi,z})}{2}D^{+}_{\tau\nu}J_{\tau+1}(\alpha_{\tau\nu}r)\right]e^{i(\tau-1)\phi}e^{i\beta z}. \tag{C18}$$

The adjoint mode is calculated as

$$\begin{aligned}\boldsymbol{E}^{\dagger}_{\tau\nu}=&D^{\dagger,+}_{\tau\nu}J_{\tau-1}(\alpha_{\tau\nu}r)e^{-i(\tau-1)\phi}e^{-i\beta z}\hat{\boldsymbol{e}}_{+}\\&+D^{\dagger,-}_{\tau\nu}J_{\tau+1}(\alpha_{\tau\nu}r)e^{-i(\tau+1)\phi}e^{-i\beta z}\hat{\boldsymbol{e}}_{-}\\&-i\beta L_{\tau\nu}J_{\tau}(\alpha_{\tau\nu}r)e^{-i\tau\phi}e^{-i\beta z},\end{aligned} \tag{C19}$$

where

$$D^{\dagger,+}_{\tau\nu}=D^{-}_{\tau\nu}\qquad D^{\dagger,-}_{\tau\nu}=D^{+}_{\tau\nu}. \tag{C20}$$

3. Integration

We note that in the rotational basis, the forms of the transverse and longitudinal modes are equivalent if we interchange $D^{-}_{\tau\nu}$ with C^{-}_{τ}, $D^{+}_{\tau\nu}$ with C^{+}_{τ}, $i\beta L_{\tau\nu}$ with C^{E}_{τ}. So, the following derivation is still valid if the modes are longitudinal or transverse. We can then proceed to the dot product in the integrand of Eq. (C1), knowing that

$$\hat{\boldsymbol{e}}_{+}\cdot\hat{\boldsymbol{e}}_{-}=1,\quad \hat{\boldsymbol{e}}_{+}\cdot\hat{\boldsymbol{e}}_{+}=\hat{\boldsymbol{e}}_{-}\cdot\hat{\boldsymbol{e}}_{-}=0. \tag{C21}$$

Thus,

$$\tilde{\boldsymbol{E}}^{\dagger}_{\nu}\cdot\Delta\overleftrightarrow{\varepsilon}\tilde{\boldsymbol{E}}_{\tau}=\tilde{E}^{\dagger,-}_{\nu}\tilde{E}^{+}_{\tau}+\tilde{E}^{\dagger,+}_{\nu}\tilde{E}^{-}_{\tau}+\tilde{E}^{\dagger,z}_{\nu}\tilde{E}^{z}_{\tau}. \tag{C22}$$

The first two terms on the left-hand side of the Eq. (C22) are

$$\begin{aligned}\tilde{E}^{\dagger,-}_{\nu}\tilde{E}^{+}_{\tau}&=C^{\dagger,-}_{\nu}J_{\nu+1}(\alpha_{\nu}r)\left[\frac{(\varepsilon_{\rho}-\varepsilon_{\phi,z})}{2}C^{-}_{\tau}J_{\tau-1}(\alpha_{\tau}r)+\frac{(\varepsilon_{\rho}+\varepsilon_{\phi,z})}{2}C^{+}_{\tau}J_{\tau+1}(\alpha_{\tau}r)\right]e^{i(\tau+1)\phi}e^{-i(\nu+1)\phi},\\&=\left[\frac{(\varepsilon_{\rho}-\varepsilon_{\phi,z})}{2}C^{-}_{\tau}C^{\dagger,-}_{\nu}J_{\nu+1}(\alpha_{\nu}r)J_{\tau-1}(\alpha_{\tau}r)+\frac{(\varepsilon_{\rho}+\varepsilon_{\phi,z})}{2}C^{+}_{\tau}C^{\dagger,-}_{\nu}J_{\nu+1}(\alpha_{\nu}r)J_{\tau+1}(\alpha_{\tau}r)\right],\times e^{i(\tau+1)\phi}e^{-i(\nu+1)\phi}.\\\tilde{E}^{\dagger,+}_{\nu}\tilde{E}^{-}_{\tau}&=C^{\dagger,+}_{\nu}J_{\nu-1}(\alpha_{\nu}r)\left[\frac{(\varepsilon_{\rho}-\varepsilon_{\phi,z})}{2}C^{+}_{\tau}J_{\tau+1}(\alpha_{\tau}r)+\frac{(\varepsilon_{\rho}+\varepsilon_{\phi,z})}{2}C^{-}_{\tau}J_{\tau-1}(\alpha_{\tau}r)\right]e^{i(\tau-1)\phi}e^{-i(\nu-1)\phi}\\&=\left[\frac{(\varepsilon_{\rho}-\varepsilon_{\phi,z})}{2}C^{+}_{\tau}C^{\dagger,+}_{\nu}J_{\nu-1}(\alpha_{\nu}r)J_{\tau+1}(\alpha_{\tau}r)+\frac{(\varepsilon_{\rho}+\varepsilon_{\phi,z})}{2}C^{-}_{\tau}C^{\dagger,+}_{\nu}J_{\nu-1}(\alpha_{\nu}r)J_{\tau-1}(\alpha_{\tau}r)\right]\times e^{i(\tau-1)\phi}e^{-i(\nu-1)\phi}.\end{aligned}$$

Finally, the last term of Eq. (C22) is

$$\tilde{E}^{\dagger,z}_{\nu}\tilde{E}^{z}_{\tau}=C^{E}_{\nu}C^{E}_{\tau}J_{\nu}(\alpha_{\nu}r)J_{\tau}(\alpha_{\tau}r)e^{-i\nu\phi}e^{i\tau\phi}. \tag{C23}$$

We integrate Eq. (C22) over the cross section of the cylinder, i.e.,

$$\iint\tilde{\boldsymbol{E}}^{\dagger}_{\nu}\cdot\Delta\overleftrightarrow{\varepsilon}\tilde{\boldsymbol{E}}_{\tau}=\int_{0}^{a}\int_{0}^{2\pi}(\tilde{E}^{\dagger,-}_{\nu}\tilde{E}^{+}_{\tau}+\tilde{E}^{\dagger,+}_{\nu}\tilde{E}^{-}_{\tau}+\tilde{E}^{\dagger,z}_{\nu}\tilde{E}^{z}_{\tau})rd\phi dr. \tag{C24}$$

In Eq. (C24), we separate the integrals over the r and θ. The angular integrals are identically zero except for $n=m$. Therefore, we can rewrite Eq. (C24) as

$$\begin{aligned}\iint\tilde{\boldsymbol{E}}^{\dagger}_{\nu}\cdot\Delta\overleftrightarrow{\varepsilon}\tilde{\boldsymbol{E}}_{\tau}=&\frac{(\varepsilon_{\rho}-\varepsilon_{\phi,z})}{2}C^{-}_{\tau}C^{\dagger,-}_{\nu}I_{\nu+1,\tau-1}(\alpha_{\tau},\alpha_{\nu},a)+\frac{(\varepsilon_{\rho}+\varepsilon_{\phi,z})}{2}C^{+}_{\tau}C^{\dagger,-}_{\nu}I_{\nu+1,\tau+1}(\alpha_{\tau},\alpha_{\nu},a)\\&+\frac{(\varepsilon_{\rho}-\varepsilon_{\phi,z})}{2}C^{+}_{\tau}C^{\dagger,+}_{\nu}I_{\nu-1,\tau+1}(\alpha_{\tau},\alpha_{\nu},a)+\frac{(\varepsilon_{\rho}+\varepsilon_{\phi,z})}{2}C^{-}_{\tau}C^{\dagger,+}_{\nu}I_{\nu-1,\tau-1}(\alpha_{\tau},\alpha_{\nu},a)+\varepsilon_{\phi,z}C^{E}_{\nu}C^{E}_{\tau}I_{\tau,\tau}(\alpha_{\tau},\alpha_{\nu},a),\end{aligned} \tag{C25}$$

where $I_{\nu,\tau}(\alpha_1,\alpha_2,a)=2\pi\int_0^a rJ_{\nu}(\alpha_1 r)J_{\tau}(\alpha_2 r)dr$.

APPENDIX D: THE INCIDENT PLANE WAVE

We consider a plane wave incident on the cylinder in the direction $k=\beta\hat{\boldsymbol{z}}+\alpha\hat{\boldsymbol{x}}$. The electric field can be written as

$$\boldsymbol{E}_{0}=(E^{x}_{0}\hat{\boldsymbol{x}}+E^{y}_{0}\hat{\boldsymbol{y}}+E^{z}_{0}\hat{\boldsymbol{z}})e^{i(\alpha r\cos\phi+\beta z)}, \tag{D1}$$

Published under license by AIP Publishing.

where $E_0^y = 0$ for p-polarized incident wave, and $E_0^x = E_0^z = 0$ for s-polarization. In the cylindrical basis of vectors, it is rewritten as

$$\boldsymbol{E}_0 = (E_0^x \cos\phi + E_0^y \sin\phi)\hat{\boldsymbol{e}}_\rho e^{i(\alpha r\cos\phi+\beta z)} + (-E_0^x \sin\phi + E_0^y \cos\phi)\hat{\boldsymbol{e}}_\phi e^{i(\alpha r\cos\phi+\beta z)} + E_0^z\hat{\boldsymbol{z}}e^{i(\alpha r\cos\phi+\beta z)}. \tag{D2}$$

Using the Jacobi–Anger expansion[64]

$$e^{i\alpha r\cos(\phi)} = \sum_\tau i^\tau J_\tau(\alpha r)e^{i\tau\phi}, \tag{D3}$$

each mode of the plane wave expansion becomes

$$\Delta\overleftrightarrow{\varepsilon}E_0 = \sum_\tau i^\tau J_\tau(\alpha r)\left[\varepsilon_\rho(E_0^x\cos\phi + E_0^y\sin\phi)\hat{\boldsymbol{e}}_\rho + \varepsilon_{\phi,z}(-E_0^x\sin\phi + E_0^y\cos\phi)\hat{\boldsymbol{e}}_\phi + \varepsilon_{\phi,z}E_0^z\hat{\boldsymbol{z}}\right]e^{i(\tau\phi+\beta z)}. \tag{D4}$$

Therefore, by writing it in the rotational basis,

$$\Delta\overleftrightarrow{\varepsilon}E_0\cdot\hat{\boldsymbol{e}}_+ = \frac{1}{2\sqrt{2}}\sum_\tau i^\tau J_\tau(\alpha r)(\varepsilon_\rho - \varepsilon_{\phi,z})(E_0^x - iE_0^y)\times e^{i(\tau+2)\phi}e^{i\beta z} \tag{D5}$$

$$+\frac{1}{2\sqrt{2}}\sum_\tau i^\tau J_\tau(\alpha r)(\varepsilon_{\phi,z} + \varepsilon_\rho)(E_0^x + iE_0^y)\times e^{i\tau\phi}e^{i\beta z}. \tag{D6}$$

Similarly,

$$\Delta\overleftrightarrow{\varepsilon}E_0\cdot\hat{\boldsymbol{e}}_- = \frac{1}{2\sqrt{2}}\sum_\tau i^\tau J_\tau(\alpha r)(\varepsilon_{\phi,z} + \varepsilon_\rho)(E_0^x - iE_0^y)_\times e^{i\tau\phi}e^{i\beta z} + \frac{1}{2\sqrt{2}}\sum_\tau i^\tau J_\tau(\alpha r)(\varepsilon_\rho - \varepsilon_{\phi,z})(E_0^x + iE_0^y) \tag{D7}$$

$$\times e^{i(\tau-2)\phi}e^{i\beta z}. \tag{D8}$$

So, for each mode, we have to calculate the integral of product of $\tilde{\boldsymbol{E}}_\nu^\dagger$ by $\Delta\overleftrightarrow{\varepsilon}^b\boldsymbol{E}_0$,

$$\begin{aligned}\tilde{E}_\nu^{\dagger,-}E_0^+ = {}& \frac{1}{2\sqrt{2}}C_\nu^{\dagger,-}(\varepsilon_\rho - \varepsilon_{\phi,z})(E_0^x - iE_0^y)\sum_\tau i^\tau J_{\nu+1}(\alpha_\nu r)J_\tau(\alpha r)e^{-i(\nu+1)\phi}e^{i(\tau+2)\phi}\\ &+\frac{1}{2\sqrt{2}}C_\nu^{\dagger,-}(\varepsilon_{\phi,z} + \varepsilon_\rho)(E_0^x + iE_0^y)\sum_\tau i^\tau J_{\nu+1}(\alpha_\nu r)J_\tau(\alpha r)e^{-i(\nu+1)\phi}e^{i\tau\phi},\end{aligned} \tag{D9}$$

$$\begin{aligned}\tilde{E}_\nu^{\dagger,+}E_0^- = {}& \frac{1}{2\sqrt{2}}C_\nu^{\dagger,+}(\varepsilon_{\phi,z} + \varepsilon_\rho)(E_0^x - iE_0^y)\sum_\tau i^\tau J_{\nu-1}(\alpha_\nu r)J_\tau(\alpha r)e^{-i(\nu-1)\phi}e^{i\tau\phi}\\ &+\frac{1}{2\sqrt{2}}C_\nu^{\dagger,+}(\varepsilon_\rho - \varepsilon_{\phi,z})(E_0^x + iE_0^y)\sum_\tau i^\tau J_{\nu-1}(\alpha_\nu r)J_\tau(\alpha r)e^{-i(\nu-1)\phi}e^{i(\tau-2)\phi},\end{aligned} \tag{D10}$$

$$\tilde{E}_\nu^{\dagger,z}E_0^z = C_\nu^E\varepsilon_{\phi,z}E_0^z\sum_\tau i^\tau J_\nu(\alpha_\nu r)J_\tau(\alpha r)e^{-i\nu\phi}e^{i\tau\phi}. \tag{D11}$$

Published under license by AIP Publishing.

The integral is then,

$$\int_0^a\int_0^{2\pi}\tilde{E}_\nu^{\dagger,-}E_0^+ rd\phi dr = i^{\nu-1}C_\nu^{\dagger,-}\frac{\varepsilon_\rho-\varepsilon_{\phi,z}}{2}\frac{E_0^x-iE_0^y}{\sqrt{2}}I_{\nu+1,\nu-1}(\alpha_\nu,\alpha,a) + i^{\nu+1}C_\nu^{\dagger,-}\frac{\varepsilon_\rho+\varepsilon_{\phi,z}}{2}\frac{E_0^x+iE_0^y}{\sqrt{2}}I_{\nu+1,\nu+1}(\alpha_\nu,\alpha,a), \tag{D12}$$

$$\int_0^a\int_0^{2\pi}\tilde{E}_\nu^{\dagger,+}E_0^- rd\phi dr = i^{\nu-1}C_\nu^{\dagger,+}\frac{\varepsilon_{\phi,z}+\varepsilon_\rho}{2}\frac{E_0^x-iE_0^y}{\sqrt{2}}I_{\nu-1,\nu-1}(\alpha_\nu,\alpha,a) + i^{\nu+1}C_\nu^{\dagger,+}\frac{\varepsilon_\rho-\varepsilon_{\phi,z}}{2}\frac{E_0^x+iE_0^y}{\sqrt{2}}I_{\nu-1,\nu+1}(\alpha_\nu,\alpha,a), \tag{D13}$$

$$\int_0^a\int_0^{2\pi}\tilde{E}_\nu^{\dagger,z}E_0^z rd\theta dr = \varepsilon_\rho i^\nu C_\nu^E E_0^z I_{\nu,\nu}(\alpha_\nu,\alpha,a). \tag{D14}$$

DATA AVAILABILITY

The data that support the findings of this study are available from the corresponding author upon reasonable request.

REFERENCES

[1]J. Yao, X. Yang, X. Yin, G. Bartal, and X. Zhang, "Three-dimensional nanometer-scale optical cavities of indefinite medium," Proc. Natl. Acad. Sci. U.S.A. **108**, 11327–11331 (2011).

[2]X. Yang, J. Yao, J. Rho, X. Yin, and X. Zhang, "Experimental realization of three-dimensional indefinite cavities at the nanoscale with anomalous scaling laws," Nat. Photonics **6**, 450–454 (2012).

[3]C. Wu, A. Salandrino, X. Ni, and X. Zhang, "Electrodynamical light trapping using whispering-gallery resonances in hyperbolic cavities," Phys. Rev. X **4**, 021015 (2014).

[4]K. Feng, G. Harden, D. L. Sivco, and A. J. Hoffman, "Subdiffraction confinement in all-semiconductor hyperbolic metamaterial resonators," ACS Photonics **4**, 1621–1626 (2017).

[5]M. R. Shcherbakov, S. Liu, V. V. Zubyuk, A. Vaskin, P. P. Vabishchevich, G. Keeler, T. Pertsch, T. V. Dolgova, I. Staude, I. Brener, and A. A. Fedyanin, "Ultrafast all-optical tuning of direct-gap semiconductor metasurfaces," Nat. Commun. **8**, 17 (2017).

[6]N. Nookala, J. Lee, M. Tymchenko, J. Sebastian Gomez-Diaz, F. Demmerle, G. Boehm, K. Lai, G. Shvets, M.-C. Amann, A. Alu, and M. Belkin, "Ultrathin gradient nonlinear metasurface with a giant nonlinear response," Optica **3**, 283 (2016).

[7]D. Bergman, "The dielectric constant of a simple-cubic array of identical spheres," J. Phys. C **12**, 4947 (1979).

[8]T. C. Choy, *Effective Medium Theory: Principles and Applications* (Oxford University Press, 2015).

[9]S. N. Samaddar, "Scattering of plane waves from an infinitely long cylinder of anisotropic materials at oblique incidence with an application to an electronic scanning antenna," Appl. Sci. Res. Sect. B **10**, 385–411 (1962).

[10]J. Monzon and N. Damaskos, "Two-dimensional scattering by a homogeneous anisotropic rod," IEEE Trans. Antennas Propag. **34**, 1243–1249 (1986).

[11]J. Monzon, "Three-dimensional scattering by an infinite homogeneous anisotropic circular cylinder: A spectral approach," IEEE Trans. Antennas Propag. **35**, 670–682 (1987).

[12]R.-B. Wu and C. H. Chen, "Variational reaction formulation of scattering problem for anisotropic dielectric cylinders," IEEE Trans. Antennas Propag. **34**, 640–645 (1986).

[13]J. C. Monzon, "On a surface integral representation for homogeneous anisotropic regions: Two-dimensional case," IEEE Trans. Antennas Propag. **36**, 1401–1406 (1988).

[14]B. Beker and K. Umashankar, "Analysis of electromagnetic scattering by arbitrarily shaped two-dimensional anisotropic objects: Combined field surface integral equation formulation," Electromagnetics **9**, 215–229 (1989).

[15]N. Uzunoglu, P. Cottis, and J. Fikioris, "Excitation of electromagnetic waves in a gyroelectric cylinder," IEEE Trans. Antennas Propag. **33**, 90–99 (1985).

[16]V. V. Varadan, A. Lakhtakia, and V. K. Varadan, "Scattering by three-dimensional anisotropic scatterers," IEEE Trans. Antennas Propag. **37**, 800–802 (1989).

[17]R. D. Graglia and P. Uslenghi, "Electromagnetic scattering from anisotropic materials, part I: General theory," IEEE Trans. Antennas Propag. **32**, 867–869 (1984).

[18]R. D. Graglia, P. L. E. Uslenghi, and R. S. Zich, "Moment method with isoparametric elements for three-dimensional anisotropic scatterers," Proc. IEEE **77**, 750–760 (1989).

[19]C. M. Rappaport and E. B. Smith, "Anisotropic FDFD computed on conformal meshes," IEEE Trans. Magn. **27**, 3848–3851 (1991).

[20]W. Sun and C. A. Balanis, "Edge-based FEM solution of scattering from inhomogeneous and anisotropic objects," IEEE Trans. Antennas Propag. **42**, 627–632 (1994).

[21]X. B. Wu and K. Yasumoto, "Three-dimensional scattering by an infinite homogeneous anisotropic circular cylinder: An analytical solution," J. Appl. Phys. **82**, 1996–2003 (1997).

[22]W. Ren, "Contributions to the electromagnetic wave theory of bounded homogeneous anisotropic media," Phys. Rev. E **47**, 664–673 (1993).

[23]E. A. Muljarov, W. Langbein, and R. Zimmermann, "Brillouin–Wigner perturbation theory in open electromagnetic systems," Europhys. Lett. **92**, 50010 (2010).

[24]P. T. Leung, S. Y. Liu, S. S. Tong, and K. Young, "Time-independent perturbation theory for quasinormal modes in leaky optical cavities," Phys. Rev. A **49**, 3068–3073 (1994).

[25]P. Lalanne, W. Yan, K. Vynck, C. Sauvan, and J.-P. Hugonin, "Light interaction with photonic and plasmonic resonances," Laser Photon. Rev. **12**, 1700113 (2018).

[26]R. Sammut and A. W. Snyder, "Leaky modes on a dielectric waveguide: Orthogonality and excitation," Appl. Opt. **15**, 1040–1044 (1976).

[27]E. A. Muljarov and W. Langbein, "Resonant-state expansion of dispersive open optical systems: Creating gold from sand," Phys. Rev. B **93**, 075417 (2016).

[28]C. Sauvan, J. P. Hugonin, I. S. Maksymov, and P. Lalanne, "Theory of the spontaneous optical emission of nanosize photonic and plasmon resonators," Phys. Rev. Lett. **110**, 237401 (2013).

[29]E. A. Muljarov and T. Weiss, "Resonant-state expansion for open optical systems: Generalization to magnetic, chiral, and bi-anisotropic materials," Opt. Lett. **43**, 1978–1981 (2018).

[30]R. Colom, R. McPhedran, B. Stout, and N. Bonod, "Modal expansion of the scattered field: Causality, nondivergence, and nonresonant contribution," Phys. Rev. B **98**, 085418 (2018).

[31]M. I. Abdelrahman and B. Gralak, "Completeness and divergence-free behavior of the quasi-normal modes using causality principle," OSA Continuum **1**, 340 (2018).

[32]P. Y. Chen, D. J. Bergman, and Y. Sivan, "Generalizing normal mode expansion of electromagnetic Green's tensor to open systems," Phys. Rev. Appl. **11**, 044018 (2019).

[33]D. J. Bergman and D. Stroud, "Theory of resonances in the electromagnetic scattering by macroscopic bodies," Phys. Rev. B **22**, 3527–3539 (1980).

[34]C. Forestiere, G. Gravina, G. Miano, M. Pascale, and R. Tricarico, "Electromagnetic modes and resonances of two-dimensional bodies," Phys. Rev. B **99**, 155423 (2019).

Published under license by AIP Publishing.

[35]M. S. Agranovich, B. Z. Katsenelenbaum, A. N. Sivov, and N. N. Voitovich, *Generalized Method of Eigenoscillations in Diffraction Theory* (Wiley-VCH, 1999).
[36]A. Farhi and D. J. Bergman, "Analysis of a Veselago lens in the quasistatic regime," Phys. Rev. A **90**, 013806 (2014).
[37]D. J. Bergman and K.-J. Dunn, "Bulk effective dielectric constant of a composite with a periodic microgeometry," Phys. Rev. B **45**, 13262–13271 (1992).
[38]M. I. Stockman, "Spaser action, loss compensation, and stability in plasmonic systems with gain," Phys. Rev. Lett. **106**, 156802 (2011).
[39]O. Schnitzer, V. Giannini, S. A. Maier, and R. V. Craster, "Surface plasmon resonances of arbitrarily shaped nanometallic structures in the small-screening length limit," Proc. R. Soc. A **472**, 20160258 (2016).
[40]K. N. Reddy, P. Y. Chen, A. I. Fernández-Domínguez, and Y. Sivan, "Revisiting the boundary conditions for second-harmonic generation at metal-dielectric interfaces," J. Opt. Soc. Am. B **34**, 1824–1832 (2017).
[41]C. Forestiere, G. Miano, G. Rubinacci, A. Tamburrino, R. Tricarico, and S. Ventre, "Volume integral formulation for the calculation of material independent modes of dielectric scatterers," IEEE Trans. Antennas Propag. **66**, 2505–2514 (2018).
[42]P. Y. Chen, Y. Sivan, and E. A. Muljarov, "An efficient solver for the generalized normal modes of non-uniform open optical resonators," J. Comput. Phys. **422**, 109754 (2020).
[43]P. Y. Chen and Y. Sivan, "Robust location of optical fiber modes via the argument principle method," Comput. Phys. Commun. **214**, 105–116 (2017).
[44]P. Y. Chen, D. J. Bergman, and Y. Sivan, "Spectral decomposition of the Lippmann–Schwinger equation applied to cylinders," arXiv:1705.01747[physics] (2017).
[45]G. Rosolen, B. Maes, P. Y. Chen, and Y. Sivan, "Overcoming the bottleneck for quantum computations of complex nanophotonic structures: Purcell and Förster resonant energy transfer calculations using a rigorous mode-hybridization method," Phys. Rev. B **101**, 155401 (2020).
[46]C. Forestiere and G. Miano, "Material-independent modes for electromagnetic scattering," Phys. Rev. B **94**, 201406 (2016).
[47]Y. Kantor and D. J. Bergman, "Elastostatic resonances—A new approach to the calculation of the effective elastic constants of composites," J. Mech. Phys. Solids **30**, 355–376 (1982).
[48]M. Pascale, G. Miano, R. Tricarico, and C. Forestiere, "Full-wave electromagnetic modes and hybridization in nanoparticle dimers," Sci. Rep. **9**, 1–21 (2019).
[49]H. Kettunen, H. Wallén, and A. Sihvola, "Tailoring effective media by Mie resonances of radially-anisotropic cylinders," Photonics **2**, 509–526 (2015).
[50]H. L. Chen and L. Gao, "Anomalous electromagnetic scattering from radially anisotropic nanowires," Phys. Rev. A **86**, 033825 (2012).
[51]P. Y. Chen and Y. Sivan, "Resolving the Gibbs phenomenon via a discontinuous basis in a mode solver for open optical systems," J. Comput. Phys. **TBA**, TBA (2020).
[52]A. Poddubny, I. Iorsh, P. Belov, and Y. S. Kivshar, "Hyperbolic metamaterials," Nat. Photonics **7**, 948–957 (2013).
[53]P. Huo, S. Zhang, Y. Liang, Y. Lu, and T. Xu, "Hyperbolic metamaterials and metasurfaces: Fundamentals and applications," Adv. Opt. Mater. **7**, 1801616 (2019).
[54]A. D. Rakić, A. B. Djurišić, J. M. Elazar, and M. L. Majewski, "Optical properties of metallic films for vertical-cavity optoelectronic devices," Appl. Opt. **37**, 5271–5283 (1998).
[55]T. Siefke, S. Kroker, K. Pfeiffer, O. Puffky, K. Dietrich, D. Franta, I. Ohlídal, A. Szeghalmi, E.-B. Kley, and A. Tünnermann, "Materials pushing the application limits of wire grid polarizers further into the deep ultraviolet spectral range," Adv. Opt. Mater. **4**, 1780–1786 (2016).
[56]P. Shekhar, J. Atkinson, and Z. Jacob, "Hyperbolic metamaterials: Fundamentals and applications," Nano Convergence **1**, 14 (2014).
[57]Special attention is given in the eigensolver routine of Eq. (5). Depending on the case that is being treated, pre-arrangement of the matrix of overlap integrals ease the calculation. In our case, since the permittivity tensor (9) is diagonal, there is no mode mixing between modes of different azimuthal orders (see Appendix C). Thus, we can re-arrange the matrix of overlap integrals to be block diagonal and solve Eq. (5) for each azimuthal order independently.
[58]In other words, higher order longitudinal modes continue to contribute significantly to the expansion. This is because the permittivity is singular at the center of the cylinder, so the electric field tends to infinity, which is difficult to represent via a linear combination of modes that are everywhere finite. Thus, we only achieve up to -18 accuracy at this point, even when including longitudinal modes up to 100th radial order.
[59]R. Kumar and K. Kajikawa, "Superscattering from cylindrical hyperbolic metamaterials in the visible region," Opt. Express **28**, 1507–1517 (2020).
[60]C. Qian, X. Lin, Y. Yang, F. Gao, Y. Shen, J. Lopez, I. Kaminer, B. Zhang, E. Li, M. Soljačić, and H. Chen, "Multifrequency superscattering from subwavelength hyperbolic structures," ACS Photonics **5**, 1506–1511 (2018).
[61]N. Maccaferri, Y. Zhao, T. Isoniemi, M. Iarossi, A. Parracino, G. Strangi, and F. De Angelis, "Hyperbolic meta-antennas enable full control of scattering and absorption of light," Nano Lett. **19**, 1851–1859 (2019).
[62]M. Kerker, D.-S. Wang, and C. L. Giles, "Electromagnetic scattering by magnetic spheres," J. Opt. Soc. Am. **73**, 765 (1983).
[63]W. Liu and Y. S. Kivshar, "Generalized Kerker effects in nanophotonics and meta-optics (invited)," Opt. Express **26**, 13085 (2018).
[64]M. Born and E. Wolf, *Principle of Optics*, 7th ed. (Cambridge, 1999).
[65]P.-H. Tsao, "Derivation and implications of the symmetry property of the permittivity tensor," Am. J. Phys. **61**, 823–825 (1993).
[66]J. A. Kong, "Theorems of bianisotropic media," Proc. IEEE **60**, 1036–1046 (1972).
[67]A. Villeneuve and R. Harrington, "Reciprocity relationships for gyrotropic media," IRE Trans. Microwave Theor. Tech. **6**, 308–310 (1958).
[68]P. S. Pershan, "Magneto-optical effects," J. Appl. Phys. **38**, 1482–1490 (1967).

Published under license by AIP Publishing.